Turkish Journal of Engineering & Environmental Sciences

http://journals.tubitak.gov.tr/engineering/

Research Article

Turkish J Eng Env Sci
(2014) 38: 363 – 372

doi:10.3906/muh-1403-12

Corrosion behavior of Ce-oxide/hydroxide coated AA7075-T6 prepared by dip immersion method

Iman DANAEE*, Maryam KANAANI, Mohammad Hosein MADDAHY, Soudabeh NIKMANESH
Abadan Faculty of Petroleum Engineering, Petroleum University of Technology, Abadan, Iran

Received: 31.03.2014 • **Accepted/Published Online:** 28.08.2015 • **Printed:** 04.03.2016

Abstract: In this study, cerium-based conversion coating was deposited on aluminum 7075-T6 by dip immersion method. Cerium oxide/hydroxide is an environmentally friendly conversion coating. Its corrosion resistance in 3.5 wt.% NaCl solution was investigated by means of electrochemical impedance spectroscopy, potentiodynamic polarization, and surface techniques. The coated samples showed a significant decrease in corrosion rate and the coating resistance increased with increasing immersion time up to 1200 s. In addition, electrochemical impedance data showed that in the presence of cerium oxide/hydroxide conversion coatings, the charge transfer resistance of aluminum increased. Surface morphology and its chemical composition were analyzed by means of scanning electron microscopy and energy dispersive spectroscopy.

Key words: Aluminum 7075, cerium oxide/hydroxide coatings, impedance, corrosion, scanning electron microscopy, potentiodynamic polarization

1. Introduction

Aluminum is widely used as a structural material because of its favorable properties such as a high strength to weight ratio, corrosion resistance, and low cost [1,2] and in military and aerospace industries [1–3] owing to its low density [3,4]. Alloying of aluminum is necessary to promote it to a high strength level [1–3] and hence reduce its vulnerability to corrosion. The presence of the second phase particles in alloys leads to a potential difference between the aluminum matrix and alloy element, which results in the formation of a galvanic cell. This galvanic cell causes a decrease in aluminum's corrosion resistance, particularly against halide ions [5–7]. In the past, chromate conversion coatings have usually been employed to protect aluminum alloys against corrosion [8–13]. The highly carcinogenic and toxic [11,12] properties of hexavalent chromium compounds forced researchers to search for more benign alternatives. Amongst the various alternatives, recently rare-earth coatings, and particularly cerium, have attracted significant attention [14–18] as cerium forms a stable oxide and hydroxide film. Furthermore, cerium-based oxide hydroxide film is nontoxic and inexpensive [16–18]. The commonly employed deposition mechanism involves both the oxidation of aluminum and the reduction of H_2O_2 in the reaction [14–19]:

$$Al \rightarrow Al^{3+} + 3e \quad (1)$$

$$H_2O_2 + 2e \rightarrow 2OH \quad (2)$$

$$Ce^{3+} + OH^- + 1/2H_2O_2 \rightarrow Ce(OH)_2^{2+} \quad (3)$$

*Correspondence: danaee@put.ac.ir

$$Ce(OH)_2^{2+} + 2OH \rightarrow Ce(OH)_4 \quad (4)$$

$$Ce(OH)_4 \rightarrow CeO_2 + 2H_2O \quad (5)$$

H_2O_2 is added to the coating bath as an effective accelerator additive. The acceleration of the cerium conversion coating process may be attributed to the rapid increase in pH, in turn caused by H_2O_2 reduction in cathodic sites. Local increase of pH leads to improving the deposition of cerium oxide and cerium hydroxide [6,19]. At lower pH, according to the Pourbaix diagram, Ce(III) is more stable, so Ce(IV) reduces to Ce(III). However, in the higher pH range, Ce(IV) is more stable, particularly when oxidizing agents like O_2 or H_2O_2 are available [8]. Previous research has described in detail the effect of different deposition methods such as sol gel, brush, and spray coatings on the corrosion resistance of cerium-based conversion coatings on aluminum 7075-T6 [20–23].

The present work, on the other hand, concentrates on the experimental investigation of the electrochemical properties of 7075-T6 aluminum alloy covered with cerium obtained by dip immersion method by impedance spectroscopy and potentiodynamic polarization. Surface morphology and chemical composition of cerium-based conversion were analyzed by scanning electron microscopy (SEM) and energy dispersive spectroscopy (EDS).

2. Experimental work

2.1. Substrate preparation

For substrate preparation we followed exactly the same steps employed in an earlier work [20]. First, cerium-based conversion coating was deposited on AA7075-T6 aluminum alloy with a chemical composition of Si: 0.4, Fe: 0.4, Cu: 1.4, Mn: 0.4, Mg: 2.2, Cr: <0.5, Zn: 5.8, Ti: <0.5, and others: <0. 5 wt.%, with Al is the balance. The specimens were cut to 1 cm $\times$ 1 cm samples from larger panels. Prior to the surface pretreatment process, all samples were mounted in epoxy resin. Aluminum coupons were then mechanically abraded with abrasive papers (400–2000 mesh). The specimens were desmutted by rinsing with acetone and alkaline cleaning by soaking in a NaOH solution, followed by their acid activation in an H_2SO_4 solution. Between each sequential step of the pretreatment process the samples were rinsed with deionized water.

Pretreated samples were coated by immersion in a cerium solution at room temperature for periods ranging from 30 s to 1800 s. The coating bath contained 1 g of $CeCl_3$, 3 drops of glycerin, and 2 mL of H_2O_2 in 100 mL of deionized water. After the coating process, they were stored at room temperature in the ambient laboratory air for 24 h.

2.2. Methods

The employed methods were also borrowed from an earlier work [20] as follows. Electrochemical impedance spectroscopy (EIS) and polarization curves were employed to evaluate the corrosion behavior of cerium-based conversion coatings. The electrolyte was 3.5 wt.% NaCl solution and the solution pH was adjusted by adding hydrochloric acid or sodium hydroxide. A three-electrode cell system (PGSTAT 302N) was used for the electrochemical tests. Ag/AgCl, platinum, and AA7075 electrodes were used as the reference, counter, and working electrodes, respectively. The potential was scanned at a rate of 1 mV s^{-1}. Polarization parameters were calculated by the Tafel extrapolation method [24,25]. A frequency sweep from 100 kHz to 10 MHz was used for EIS measurements. EIS data were curve-fitted to the proposed equivalent circuit by in-house least square software based on the Marquardt method for the optimization of functions and Macdonald weighting for the real and imaginary parts of the impedance [26,27]. SEM (VEGA, TESCAN-LMU) equipped with EDS was employed to characterize the surface morphology and average chemical composition.

3. Results and discussion

3.1. Surface analysis

Figure 1a presents the cerium conversion coatings of aluminum obtained in 1200 s of immersion time in cerium solution. The cerium conversion coating exhibits a uniform surface with mud-crack morphology, and some external growth and an enriched zone are also observed on the coating surface. It has been reported that these cracks and enriched zones are results of the high precipitation rate of the cerium oxide/hydroxide layer above the intermetallics [7,28,29]. The cracks, on the other hand, were attributed to the drying process performed after the samples were taken out of the conversion bath [7]. The existence of these cracks in Figure 1 bears no strict relation with the intermetallics as they are distributed over the whole surface. Figure 1b shows the cerium conversion coating obtained with a short immersion time. Figure 1b exhibits that the quality of the conversion layer is low and the coating does not cover the whole surface. The EDX analysis of cerium conversion coating

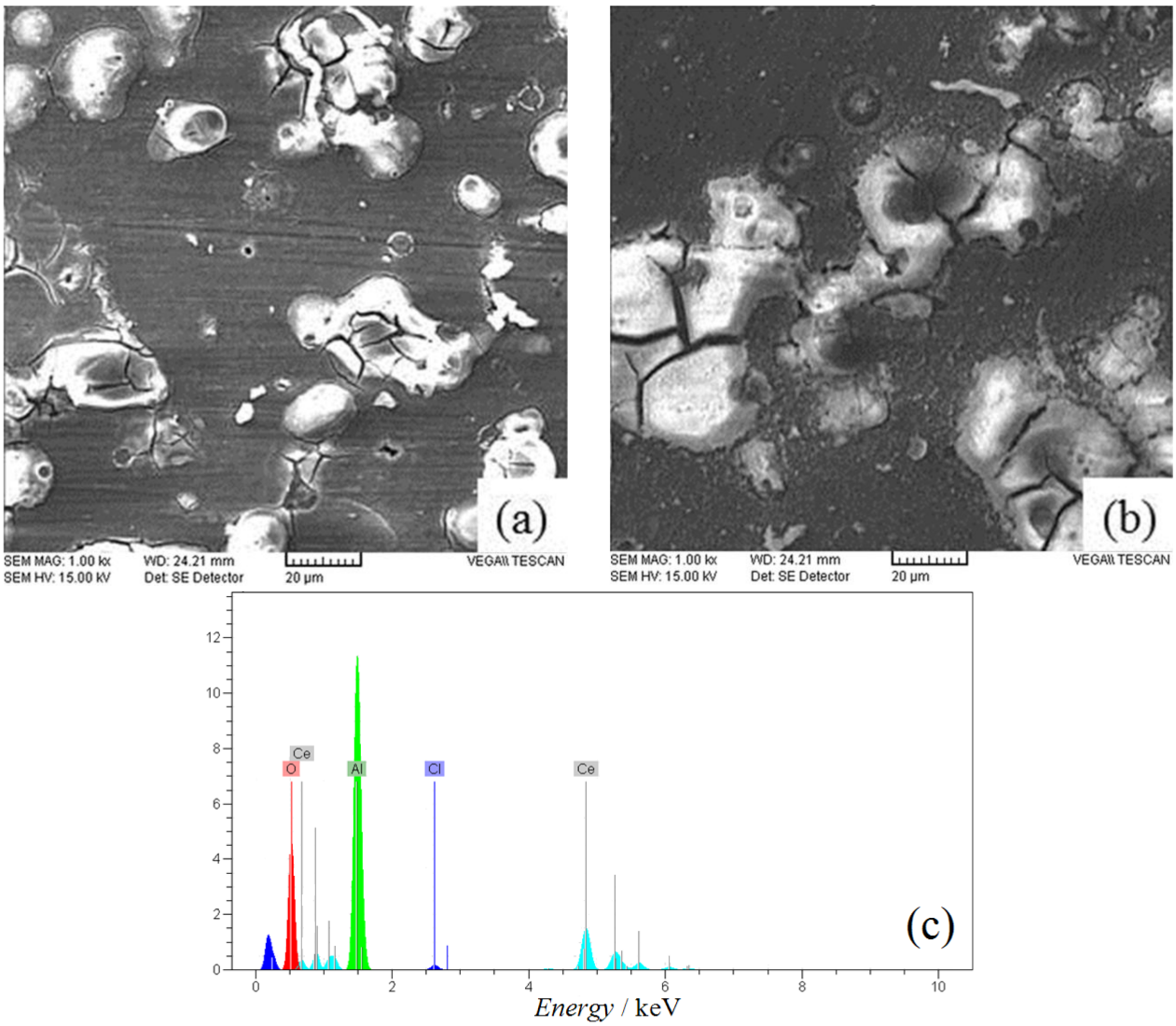

Figure 1. a) SEM micrographs of cerium conversion coated AA7075 obtained after a) 1200 s and b) 30 s immersion. c) EDX analysis of cerium oxide coating.

with a 31.2 wt.% cerium content is exhibited in Figure 1c. The precipitates formed from immersion method at room temperature consist mainly of cerium hydroxide.

3.2. Potentiodynamic polarization measurements

The electrochemical behavior of the cerium oxide/hydroxide coatings at different immersion times was investigated by potentiodynamic polarization in 3.5 wt.% NaCl solution. Polarization curves of the cerium oxide/hydroxide coated AA7075 electrode are shown in Figure 2. The anodic and cathodic polarization branches in Figure 2 demonstrate Tafel type behavior [24,25] of these samples in the active state. Table 1 exhibits the corrosion parameters such as corrosion current density (I_{corr}), corrosion potential (E_{corr}), polarization resistance (R_P), and Tafel slopes [24,25] (β_a, β_c). The polarization resistance is calculated by the following equation [30]:

$$Rp = \frac{\beta a.\beta c}{2.303(\beta a + \beta c)} \times \frac{1}{Icorr}. \tag{6}$$

According to Table 1, the corrosion current density and corrosion rate decrease in the presence of cerium oxide/hydroxide coatings. The decrease in corrosion rate indicates the barrier properties of the cerium oxide/hydroxide films on the AA7075 substrate in a corrosive environment. Table 1 also shows that by increasing immersion time from 30 to 1200 s, I_{corr} and corrosion rate of the coated samples decrease. With the increase of immersion time up to 1200 s, propagation of cerium oxide/hydroxide on the surface increases and covers the entire surface (Figure 1). After withdrawing samples from the solution and drying them at ambient temperature, cracks on their surface propagate and decrease the corrosion resistance of the coatings. The upper layer of the coating will be hardened during drying, trapping the water in the inner cerium oxide/hydroxide layer. It is the trapped water that cannot escape from the coating that leads to cracking. After 1200 s of immersion time, both corrosion current density and corrosion rate increase, which is related to the formation of deep cracks within thick film and hence a decrease in coated sample toughness.

Table 1. Potentiodynamic polarization parameters for the corrosion of cerium oxide coated aluminum in 3.5 wt.% NaCl solution as a function of different immersion times.

Immersion time	E_{corr} mV	I_{corr} A cm^2	β_aV dec^{-1}	$-\beta_c$V dec^{-1}	$R_p$ohm	V_{corr} mm year^{-1}
0 (bare)	–546	1.32×10^{-6}	0.051	0.556	1.53×10^{4}	1.55×10^{-2}
30 s	–511	6.40×10^{-7}	0.057	0.335	3.33×10^{4}	7.52×10^{-3}
300 s	–538	5.02×10^{-7}	0.039	0.157	2.74×10^{4}	5.89×10^{-3}
600 s	–558	1.52×10^{-7}	0.047	0.243	1.12×10^{5}	1.79×10^{-3}
1200 s	–637	9.19×10^{-8}	0.089	0.199	2.91×10^{5}	1.08×10^{-3}
1800 s	–597	5.94×10^{-7}	0.183	0.132	5.61×10^{4}	6.97×10^{-3}

As shown in Figure 2, the corrosion resistance of coated aluminum increases up to 15–20 times in comparison to that of the bare aluminum. Valdes et al. [31] demonstrated that the corrosion resistance of aluminum alloy 6061 increases in the presence of cerium-based coatings deposited by immersion method. They also showed that despite the presence of some cracks in the coatings, the corrosion resistance increased up to 20–30 times. Earlier literature claimed that higher corrosion-resistant coating can be obtained by other coatings methods [32,33]. However, the existence of such cracks was also seen in these methods, like spraying [32–35]. Note that the dip immersion is a simple and inexpensive method in comparison with other methods.

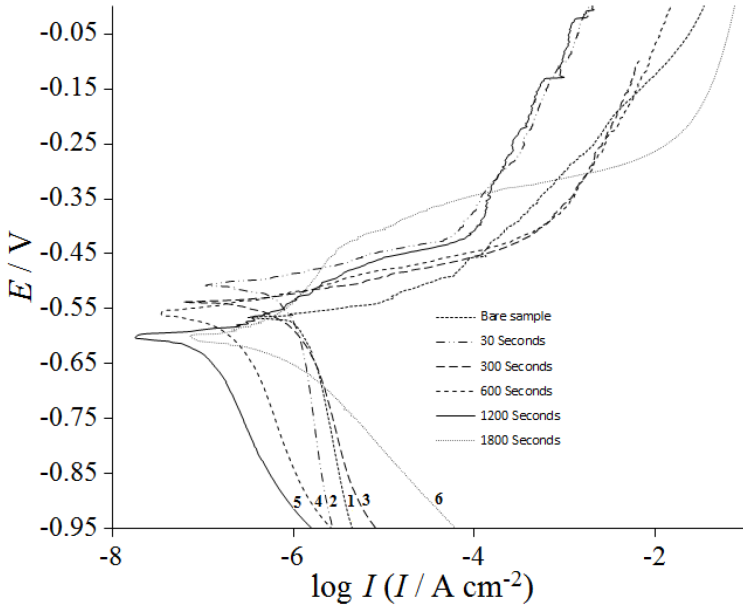

Figure 2. Potentiodynamic polarization curves of cerium-coated AA7075 in 3.5 wt.% NaCl solution, where cerium conversion was obtained for different immersion times: 1) bare, 2) 30 s, 3) 300 s, 4) 600 s, 5) 1200 s, and 6) 1800 s.

Table 1 shows that the cerium-coated sample immersed in a bath for 1200 s forms a more protective layer on the aluminum surface. The influence of cerium-based conversion coating is more pronounced in the cathodic polarization plots compared to that of the anodic polarization plots in Figure 2. Such behavior is evidence of cerium deposition as an oxide/hydroxide on cathodic sites, which prevents the cathodic reaction [36]. Apparently, the anodic reactions are balanced by cathodic reactions on the metal surface. Cerium deposition occurs due to local pH increase produced by the cathodic reaction of H_2O_2 near the intermetallic compounds [23].

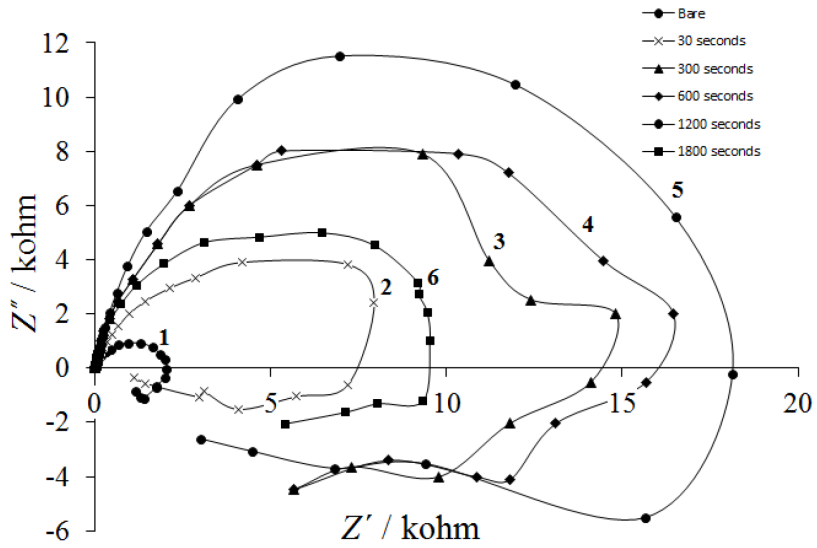

Figure 3. Impedance diagrams of cerium oxide coated aluminum 7075 in 3.5 wt.% NaCl solution where cerium coating was obtained for different immersion times in cerium chloride solutions: 1) bare, 2) 30 s, 3) 300 s, 4) 600 s, 5) 1200 s, and 6) 1800 s.

3.3. Electrochemical impedance

The electrochemical impedance property was employed to confirm the anticorrosion behavior of the cerium coating. Figure 3 presents the impedance diagrams of cerium conversion coated AA7075 obtained in different immersion times in a cerium bath. Impedance was measured at open circuit potential in a 3.5 %wt. NaCl solution. In Figure 3, two distinct semicircles are visible in high- and low-frequency ranges for each sample. The high-frequency domain loop can be attributed to metal dissolution and formation of oxide film on the surface, whereas the low-frequency loop can be ascribed to inductive nature due to accumulation of ionic chloride in the vicinity of the metal surface. The equivalent circuit compatible with the Nyquist diagram is depicted in Figure 4. The simplest approach requires the theoretical transfer function $Z\ (\omega)$ to be represented by [37]:

$$Z(\omega) = Rs\ + \frac{iwR_{ct}L + R_{ct}R_L}{R_{ct} + R_L + iwL + R_{ct}R_LQ_{dl}\,(iw)^n + R_{ct}LQ_{dl}\,(iw)^{n+1}}, \tag{7}$$

where w is the frequency in rad/s, $w = 2\pi f$, and f is frequency in Hz. In this electrical equivalent circuit, R_s, Q_{dl}, and R_{ct} represent solution resistance, a constant phase element corresponding to the double layer capacitance $Q_{dl} = R^{n-1}C_{dl}^n$, and the charge transfer resistance. R_L is the inductor's resistance and L is inductance in the low-frequency range of impedance. To obtain a satisfactory impedance simulation of cerium oxide/hydroxide coated aluminum, it is necessary to replace the capacitor (C) with a constant phase element (CPE) Q in the equivalent circuit. The presence of CPE behavior and depressed semicircles on solid electrodes is mostly attributed to microscopic roughness, which causes an inhomogeneous distribution in the solution resistance as well as in the double-layer capacitance [38,39].

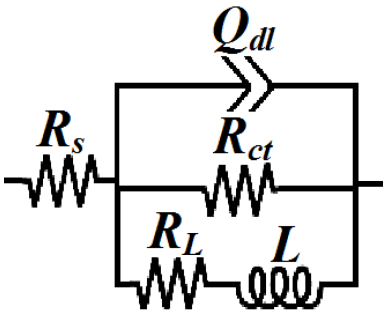

Figure 4. Equivalent circuits compatible with the experimental impedance data in Figure 2 for corrosion of cerium oxide coated aluminum electrode.

An equivalent circuit has been corroborated by inferring its parameters from curve-fitting of the experimental data to equivalent circuit values. Table 2 lists the equivalent circuit parameters for the impedance spectra of corrosion of cerium oxide/hydroxide coated aluminum in NaCl solution. Table 2 shows that the charge transfer resistance increases with increasing immersion time in coating solution. The increase in the resistance is due to the presence of the more adherent and uniform cerium coating on the surface of AA7075, which decreases the active area of the substrate. However, once the immersion time reaches and exceeds 1800 s, a slow decrease in the impedance follows owing to the formation of larger cracks.

The Q_{dl} exponent (n) is a measure of the surface heterogeneity and its increasing values indicate that the aluminum surface becomes more homogeneous with increasing immersion time as a result of uniform coatings and corrosion inhibition.

Table 2. Equivalent circuit parameters for the corrosion of cerium oxide coated aluminum in 3.5 wt.% NaCl solution obtained for different immersion times in cerium solutions.

Sample	R_s Ω	$R_{ct} \times 10^{-4}$ Ω	$Q_{dl} \times 10^4$ F	n	$R_L \times 10^{-3}$ Ω	$\boldsymbol{L} \times 10^{-5}$ H
0 (bare)	5.5	0.21	20	0.88	0.7	3
30 s	6.5	0.81	1	0.93	2.8	2
300 s	6	1.51	1	0.96	13	5
600 s	6	1.72	2	0.96	19	6.5
1200 s	6.3	1.92	1	0.98	10	5
1800 s	5.4	0.98	2	0.96	15	10

Time dependency of cerium oxide/hydroxide coated aluminum in NaCl solution is shown in Figure 5 and the corresponding impedance parameters are presented in Table 3. Cerium conversion coating was obtained by 1200 s of immersion in coating solution. Figure 5 shows that the charge transfer resistance increases with increasing immersion time of up to 96 h in corrosive solutions. For long immersion times the charge transfer resistance decreases as a result of deeper penetration of Cl^- into the coating layer and deteriorates the cerium conversion coatings. In addition, the double-layer capacitance increases with increasing immersion time due to the increase of ion penetration into the coating.

Table 3. Equivalent circuit parameters for the corrosion of cerium oxide coated aluminum in 3.5 wt.% NaCl solution obtained in different immersion times in corrosive solutions. Cerium coating was obtained by 1200 s immersion in coating solutions.

Immersion time	R_s Ω	$R_{ct} \times 10^{-4}$ Ω	$Q_{dl} \times 10^4$ F	n	$R_L \times 10^{-3}$ Ω	$L \times 10^{-5}$ H
30 min	6.3	1.92	1	0.98	10	5
48 h	6	2.42	2	0.96	12	6
96 h	6.3	2.21	5	0.95	11	7
144 h	6.4	1.81	8	0.92	10	6

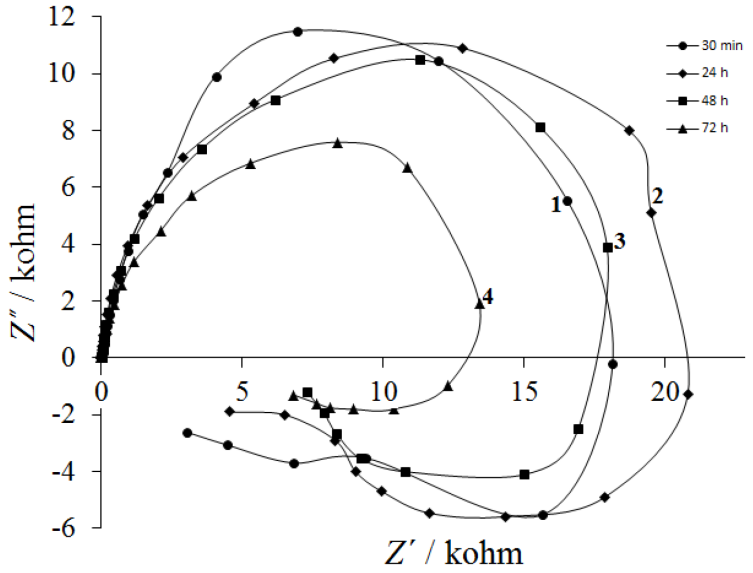

Figure 5. Impedance diagrams of cerium oxide coated aluminum 2024 with different immersion time in 3.5 wt.% NaCl solution: 1) 30 min, 2) 48 h, 3) 96 h, and 4) 144 h. Cerium coating was obtained by 1200 s of immersion in coating solutions.

4. Conclusion

Cerium oxide/hydroxide was developed as an environmentally friendly conversion coating on aluminum alloy AA7075 by dip immersion method. The electrochemical behavior of AA7075 aluminum alloy coated with cerium conversion coating was investigated in 3.5 wt.% NaCl solution by using potentiodynamic polarization, electrochemical impedance, and SEM-EDS analysis. The electrochemical behavior analysis showed that the cerium-based conversion coating improved the corrosion resistance of the alloy since it inhibited both the anodic and cathodic reaction rates in chloride-containing environments. Immersion time in the cerium solution significantly influenced the corrosion properties positively up to 1200 s and adversely beyond 1200 s, and hence the optimum coating behavior was observed at about 1200 s of immersion time. The coating produced with longer immersion times had increased corrosion rates owing to water trapping, which in turn leads to development and propagation of deep cracks.

References

[1] Arık H, Bağcı C. Investigation of influences of pressing pressure and sintering temperature on the mechanical properties of Al-Al_4C_3 composite materials. Turkish J Eng Env Sci 2003; 27: 53–58.

[2] Darmiani E, Danaee I, Golozar MA, Toroghinejad MR, Ashrafi A, Ahmadi A. Reciprocating wear resistance of Al–SiC nano-composite fabricated by accumulative roll bonding process. Materials and Design 2013; 50: 497–502.

[3] Temizel G, Özenbaş M. Intermetallic phase formation at Fe-Al film interfaces. Turkish J Eng Env Sci 2007; 31: 71–78.

[4] Bazrafshan E, Mahvi AH, Naseri S, Mesdaghinia AR. Performance evaluation of electrocoagulation process for removal of chromium (VI) from synthetic chromium solutions using iron and aluminum electrodes. Turkish J Eng Env Sci 2008; 32: 59–66.

[5] Alnıak MO, Bedir F. Changes of grain sizes and flow stresses of AA2014 and AA6063 aluminum alloys at high temperatures in various strain rates. Turkish J Eng Env Sci 2003; 27: 59–64.

[6] Darmiani E, Danaee I, Golozar MA, Toroghinejad MR. Corrosion investigation of Al–SiC nano-composite fabricated by accumulative roll bonding (ARB) process. J Alloys Comp 2013; 552: 31–39.

[7] Tan E, Ögel B. Influence of heat treatment on the mechanical properties of AA6066 alloy. Turkish J Eng Env Sci 2007; 31: 53–60.

[8] Bahri H, Danaee I, Rashed GR, Zaarei D. Effect of silica ratio on the corrosion behavior of nano-silica potassium silicate coatings on aluminum alloy 2024. J Mater Eng Perform 2015; 24: 839–847.

[9] Campestrini P, Böhm S, Schram T, Terryn H, Wit JHWD. Study of the formation of chromate conversion coatings on Alclad 2024 aluminum alloy using spectroscopic ellipsometry. Thin Solid Films 2002; 410: 76–85.

[10] Bahri H, Danaee I, Rashed GR. The effect of curing time and curing temperature on the corrosion behavior of nanosilica modified potassium silicate coatings on AA2024. Surf Coat Technol 2014; 254: 305–312.

[11] Kazemi M, Danaee I, Zaarei D. The effect of pre-anodizing on corrosion behavior of silicate conversion coating on AA2024. Mater Chem Phys 2014; 148: 223–229.

[12] Campestrini P, Westing EV, Hovestad A, Wit JD. Investigation of the chromate conversion coating on Alclad 2024 aluminium alloy: effect of the pH of the chromate bath. Electrochim Acta 2002; 47: 1097–1113.

[13] Zhao J, Xia L, Sehgal A, Lu D, McCreery RL, Frankel GS. Effects of chromate and chromate conversion coatings on corrosion of aluminum alloy 2024-T3. Surf Coat Technol 2001; 140: 51–57.

[14] Li L, Lei J, Yu S, Tian Y, Jiang Q, Pan F. Formation and characterization of cerium conversion coatings on magnesium alloy. J Rare Earths 2008; 26: 383–387.

[15] Danaee I, Zamanizadeh HR, Fallahi M, Lotfi B. The effect of surface pre-treatments on corrosion behavior of cerium-based conversion coatings on Al 7075-T6. Mater Corros 2014; 65: 815–819.

[16] Kiyota S, Valdez B, Stoytcheva M, Zlatev R, Bastidas JM. Anticorrosion behavior of conversion coatings obtained from unbuffered cerium salts solutions on AA6061-T6. J Rare Earths 2011; 29: 961–968.

[17] Aziz I, Zhang Q, Xiang M. Using EIS to evaluate anti-corrosion properties of the SiCp/5A06 aluminium MMC treated by cerium conversion coatings. J Rare Earths 2010; 28: 109–116.

[18] Zhao D, Sun J, Zhang L, Tan Y, Li J. Corrosion behavior of rare earth cerium based conversion coating on aluminum alloy. J Rare Earths 2010; 28: 371–374.

[19] Lim WF, Cheong KY, Lockman Z. Effects of post-deposition annealing temperature and time on physical properties of metal-organic decomposed lanthanum cerium oxide thin film. Thin Solid Films 2011; 519: 5139–5145.

[20] Kanani M, Danaee I, Maddahy MH. Microstructural characteristics and corrosion behavior of cerium oxide conversion coatings on AA6063. Mater Corros 2014; 65: 1073–1079.

[21] Joshi S, Kulp EA, Fahrenholtz WG, O'Keefe MJ. Dissolution of cerium from cerium-based conversion coatings on Al 7075-T6 in 0.1 M NaCl solutions. Corros Sci 2012; 60: 290–295.

[22] Johnson BY, Edington J, O'Keefe MJ. Effect of coating parameters on the microstructure of cerium oxide conversion coatings. Mater Sci Eng A 2003; 361: 225–231.

[23] De Frutos A, Arenas MA, Liu Y, Skeldon P, Thompson GE, De Damborenea J, Conde A. Influence of pre-treatments in cerium conversion treatment of AA2024-T3 and 7075-T6 alloys. Surf Coat Technol 2008; 202: 3797–3807.

[24] Shi Z, Liu M, Atrens A. Measurement of the corrosion rate of magnesium alloys using Tafel extrapolation. Corros Sci 2010; 52: 579–588.

[25] Flitt HJ, Schweinsberg DP. Evaluation of corrosion rate from polarisation curves not exhibiting a Tafel region. Corros Sci 2005; 47: 3034–3052.

[26] Danaee I. Kinetics and mechanism of palladium electrodeposition on graphite electrode by impedance and noise measurements. J Electroanal Chem 2011; 662: 415–420.

[27] Macdonald JR. Note on the parameterization of the constant-phase admittance element. Solid State Ion 1984; 13: 147–149.

[28] Hughes AE, Taylor RJ, Hinton BRW, Wilson L. XPS and SEM characterization of hydrated cerium oxide conversion coatings. Surf Interface Anal 1995; 23: 540–550.

[29] Xingwen Y, Chunan C, Zhiming Y, Derui Z, Zhongda Y. Corrosion behavior of rare earth metal (REM) conversion coatings on aluminum alloy LY12. Mater Sci Eng A 2000; 284: 56–63.

[30] Danaee I, Ghasemi O, Rashed GR, Rashvand Avei M, Maddahy MH. Effect of hydroxyl group position on adsorption behavior and corrosion inhibition of hydroxybenzaldehyde Schiff bases, electrochemical and quantum calculations. J Mol Struct 2013; 1035: 247–259.

[31] Valdez B, Kiyota S, Stoytcheva M, Zlatev R, Bastidas JM. Cerium-based conversion coatings to improve the corrosion resistance of aluminium alloy 6061-T6. Corros Sci 2014; 87: 141–149.

[32] Živković LS, Popić JP, Jegdić BV, Dohčević-Mitrović Z, Bajat JB, Mišković-Stanković VB. Corrosion study of ceria coatings on AA6060 aluminum alloy obtained by cathodic electrodeposition: effect of deposition potential. Surf Coat Technol 2014; 240: 327–335.

[33] Heller DK, Fahrenholtz WG, Keefe MJO. The effect of post-treatment time and temperature on cerium-based conversion coatings on Al 2024-T3. Corros Sci 2010; 52: 360–368.

[34] Geng S, Yu P, Keefe MJO, Fahrenholtz WG, Keefe TJO. Screening study of spray solution parameters for depositing cerium-based conversion coatings on Al alloy 2024-T3. J Appl Electrochem 2010; 40: 551–559.

[35] Pardo A, Merino MC, Arrabal R, Viejo F, Carboneras M, Muñoz JA. Influence of Ce surface treatments on corrosion behaviour of A3xx.x/SiCp composites in 3.5wt.% NaCl. Corros Sci 2006; 48: 3035–3048.

[36] Hasannejad H, Aliofkhazraei M, Shanaghi A, Shahrabi T, Sabour AR. Nanostructural and electrochemical characteristics of cerium oxide thin films deposited on AA5083-H321 aluminum alloy substrates by dip immersion and sol–gel methods. Thin Solid Film 2009; 517: 4792–4799.

[37] Danaee I, Noori S. Kinetics of the hydrogen evolution reaction on NiMn graphite modified electrode. Int J Hydrogen Energy 2011; 36: 12102–12111.

[38] Danaee I, Niknejad Khomami M, Attar AA. Corrosion behavior of AISI 4130 steel alloy in ethylene glycol–water mixture in presence of molybdate. Mater Chem Phys 2010; 135: 658–667.

[39] Jafari H, Danaee I, Eskandari H, Rashvand Avei M. Electrochemical and theoretical studies of adsorption and corrosion inhibition of N,N′-Bis(2-hydroxyethoxyacetophenone)-2,2-dimethyl-1,2-propanediimine on low carbon steel (API 5L Grade B) in acidic solution. Ind Eng Chem Res 2013; 52: 6617–6632.